

**A comparative study of force sensors for scanning probe  
microscopy based on quartz tuning forks and length extensional  
resonators.**

Franz J. Giessibl\* and Florian Pielmeier

*Universität Regensburg, Institute of Experimental and Applied Physics,  
Universitätsstrasse 31, D-93040 Regensburg, Germany.*

Toyoaki Eguchi<sup>†</sup>

*NAKAJIMA Designer Nanocluster Assembly Project, ERATO,  
Japan Science and Technology Agency (JST) 3-2-1 Sakato,  
Takatsu-ku, Kawasaki 213-0012, Japan*

*Graduate School of Science and Technology,  
Keio University 3-14-1 Hiyoshi, Kohoku-ku, Yokohama 223-8522, Japan*

Toshu An

*Institute for Materials Research, Tohoku University,  
2-1-1, Katahira, Aoba-ku, Sendai 980-8577, JAPAN*

Yukio Hasegawa

*Institute for Solid State Physics, University of Tokyo 5-1-5,  
Kashiwa-no-ha, Kashiwa, Chiba 277-8581 Japan.*

(Dated: November 30, 2018)

## Abstract

The force sensor is key to the performance of atomic force microscopy (AFM). Nowadays, most AFMs use micro-machined force sensors made from silicon, but piezoelectric quartz sensors are applied at an increasing rate, mainly in vacuum. These self sensing force sensors allow a relatively easy upgrade of a scanning tunneling microscope to a combined scanning tunneling/atomic force microscope. Two fundamentally different types of quartz sensors have achieved atomic resolution: the ‘needle sensor’ that is based on a length extensional resonator and the ‘qPlus sensor’ that is based on a tuning fork. Here, we calculate and measure the noise characteristics of these sensors. We find four noise sources: deflection detector noise, thermal noise, oscillator noise and thermal drift noise. The first three noise sources are inversely proportional to amplitude. Thermal drift noise is independent of the amplitude, proportional to the spring constant of the sensor and roughly proportional to  $1/\sqrt{f_{mod}}$ . Finally, we suggest how the signal-to-noise ratio of the sensors can be further improved and briefly discuss the challenges of mounting tips.

---

\*Electronic address: franz.giessibl@physik.uni-regensburg.de

†Electronic address: eggy@ncassembly.jst.go.jp

## I. INTRODUCTION

‘Atomic Force Microscopy’ (AFM) has been introduced in 1986 by Binnig, Gerber and Quate [1]. The large number of citations (the article is now one of the most highly cited publications that have appeared in *Physical Review Letters*) show that AFM is an important scientific tool with fruitful applications in various fields of science. The key element of AFM is the force sensor that probes the small forces that act between a sharp tip and a sample. Simplifying the force sensor and increasing its force resolution and imaging speed are therefore important tasks.

Atomic resolution by AFM on a reactive surface was first achieved by frequency modulation AFM (FM-AFM) [2] utilizing a piezo-resistive silicon cantilever[3] with a spring constant of  $k = 17\text{ N/m}$  at an oscillation amplitude of  $A = 34\text{ nm}$  [4]. While atomic resolution on various surfaces has been obtained with similar combinations of  $(k, A)$  (see table I in [5]), a calculation of the signal-to-noise ratio in FM-AFM as a function of the oscillation amplitudes yielded an optimal oscillation amplitude that corresponds to the decay length of the forces that are used for imaging. The spring constant of the cantilever should be as small as possible for obtaining a large frequency shift, on the other hand, the cantilever must be stiff enough to prevent instabilities such as jump-to-contact [6]. Compared to the ‘classic’ parameter set of  $(k, A)$ , the spring constant of the sensor has to be larger by a factor of 30 to 200, and the amplitude has to be reduced by a factor of 1/300 to 1/600. The reduced amplitude not only increases the signal-to-noise ratio, it also reduces the sensitivity to unwanted long-range force contributions [5]. Figure 1 shows the parameters used with ‘classic’ Si cantilevers, qPlus sensors and needle sensors.

For atomic imaging, it was suggested that the optimal stiffness  $k_{opt}$  is approximately in the interval

$$500\text{ N/m} < k_{opt} < 3000\text{ N/m} \quad (1)$$

at amplitudes of about 100 pm [6].

Self-sensing cantilevers such as piezo-resistive silicon cantilevers or piezo-electric quartz sensors are attractive because this eliminates the complications of deflection measurements based on electron tunneling [1] or optical means [7]. Because FM-AFM relies on the alteration of the oscillation frequency of the cantilever under the influence of tip-sample force gradients, a high intrinsic frequency stability of the cantilever is desirable. Silicon can-

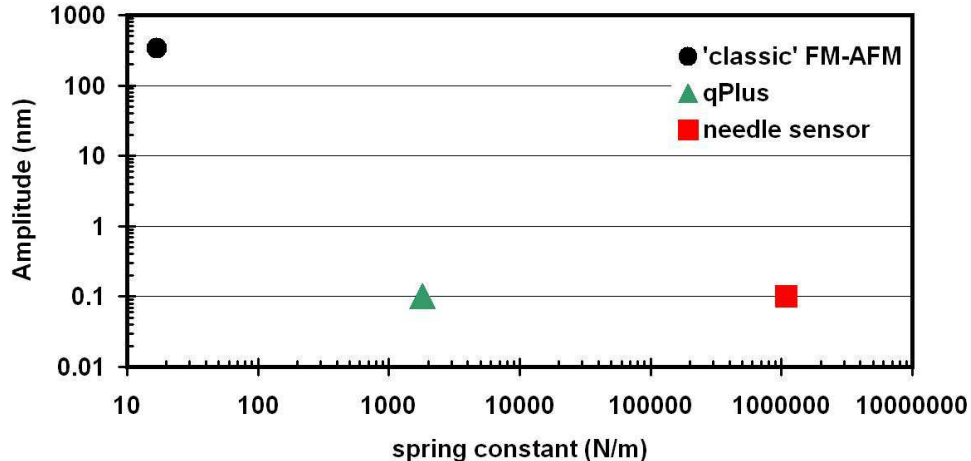


FIG. 1: Parameter fields of cantilever spring constants  $k$  and oscillation amplitudes  $A$  for classic Si cantilevers, qPlus sensors and needle sensors. To enable stable oscillation of the cantilever at the optimal amplitudes around 100 pm, it was necessary to increase the spring constants of cantilevers ('classic' FM-AFM) from about 10 N/m by more than two orders of magnitude (qPlus sensors). Here, we inquire if a further increase by almost three orders of magnitude (needle sensor) is beneficial.

tilevers, the most widespread type in use, change their frequency by  $-35$  ppm per K at room temperature [8]. In contrast, quartz resonators change their frequency by less than 1 ppm per K as long as their temperature is kept within  $\pm 14$  K of their turnover temperature (see eq. 47). The outstanding stability of quartz that has been utilized since decades for frequency standards provides for highly stable FM-AFM sensors as well.

Two types of commercially available quartz frequency standards are particularly well suited for conversion into force sensors: quartz tuning forks and length extensional resonators. Both tuning forks and length extensional resonators essentially consist of two coupled electromechanical oscillators that have exactly the same eigenfrequency and oscillate in an antiparallel mode. Attaching a tip to one of the oscillators changes its resonance frequency, so the tip either has to be very light or a similar mass has to be attached to the other oscillator. Force sensors based on tuning forks have been used by Guethner et al. [9] already in 1989, where a tip has been mounted onto one prong, and the mass of the tip was balanced with a counterweight on the other prong [10]. The length extensional

	$L$ ( $\mu\text{m}$ )	$L_e$ ( $\mu\text{m}$ )	$t$ ( $\mu\text{m}$ )	$w$ ( $\mu\text{m}$ )	$k'$ (N/m)	$k$ (N/m)	$f_0$ (Hz)
needle sensor	1340	1100	70	130	540 000	1 080 000	1 000 000
qPlus sensor	2400	1600	214	126	1 800	1 800	32 768

TABLE I: Geometrical parameters, stiffness  $k$  and eigenfrequency  $f_0$  of the quartz oscillators used. The needle sensor is based on a length extensional resonator, while the qPlus sensor is based on a quartz tuning fork.

resonator has been supplemented by a light tip on one of its two bars to form the needle sensor after Bartzke et al.[11, 12] in 1993. The qPlus sensor is also based on a tuning fork, but one of the prongs is immobilized by attaching it to a heavy substrate such that the free prong is essentially a quartz cantilever [13–15]. In this case, the tip can be massive, and the oscillating tip can interact vigorously with the sample without a reduction in the  $Q$  value. These sensors with metal probe tips allow a simple implementation of combined scanning tunneling microscopy (STM) and AFM. Quartz tuning forks are available with eigenfrequencies  $f_0$  ranging from about 32 to 200 kHz. Length extensional resonators are available in eigenfrequencies of one to a few MHz. In the comparison here, we focus on a specific type of tuning fork that is used in SWATCH wristwatches with stiffness  $k' = 1800$  N/m and  $f_0 = 32768$  Hz and a specific type of length extensional resonator with  $k' = 540$  kN/m and  $f_0 = 1$  MHz, because these types were used in the experimental data cited below (see Fig. 2 and Table I for geometric details). In section VII, we will suggest optimized geometries for both types of sensors, but here we refer to ‘standard qPlus-’ or ‘standard needle sensor’ to be based on the geometries as specified in Table I.

A qPlus sensor with  $k = 1.8$  kN/m has allowed subatomic spatial resolution [16, 17], atomic resolution of lateral forces [18], simultaneous force and current spectroscopy on graphite [19], the measurement of forces acting in atomic manipulation [21], the detection of a single charge on an atom [22] and unprecedented spatial resolution of an organic molecule [23] and helped to identify an initially unidentified organic molecule that was hauled up from the Mariana Trench [24]. Even more recent, the relationship between tunneling current and forces has been revealed [25] and the interaction of two CO molecules has been studied [26].

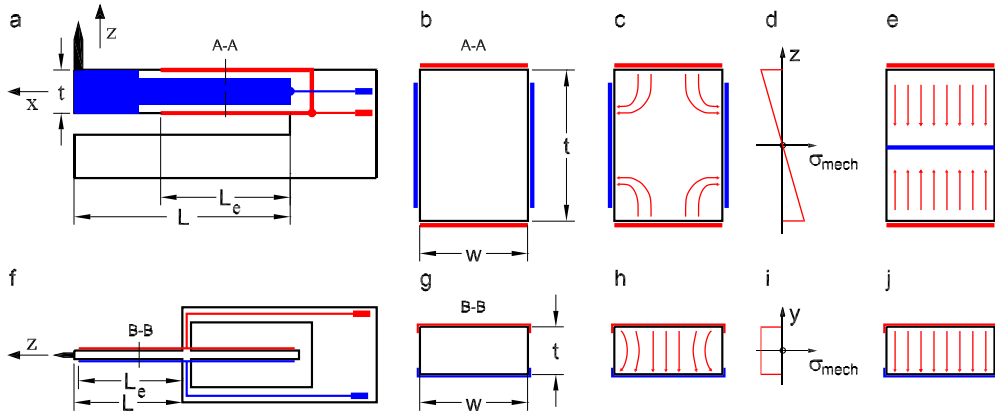


FIG. 2: Geometry of sensors based on quartz tuning forks (a-e) and length extensional resonators (f-j). A qPlus sensor (a) is created by attaching one of the prongs of the tuning fork to a substrate and attaching a tip to the other prong. For clarity, only the electrodes on the free prong are shown. The prong without displayed electrodes is fixed to a massive substrate (not shown here, see Fig. 1 in [15]). A needle sensor (f) is built by attaching a light tip to one prong of the length extensional resonator. Figures (a,b,f,g) illustrate the geometrical dimensions as listed in table I, (c,h) show a schematic view of the electrostatic field in the cross sections and (d,i) show the mechanical stress profile along a cross section. Figures (e,j) show the idealized field distribution within the quartz crystals. The qPlus sensor uses a bending mode, thus the mechanical stress is maximal where the charge-collecting electrodes are located (d), while the length extensional resonator develops a uniform stress profile (i). The idealized field distribution (e,j) is much closer to the actual field distribution (c,h) for the needle sensor (j vs. h) than for the qPlus sensor (e vs. c).

Although the needle sensor's effective stiffness of more than  $1 \text{ MN/m}$  ( $k = 2k'$ , see eq. 16) is far beyond the stiffness range that is suggested to be optimal above, it has produced atomic resolution on silicon at 4 K [28, 29] and at room temperature [30]. Therefore it is instructive to analyze the success factors of these sensors for the purpose of further improving their performance.

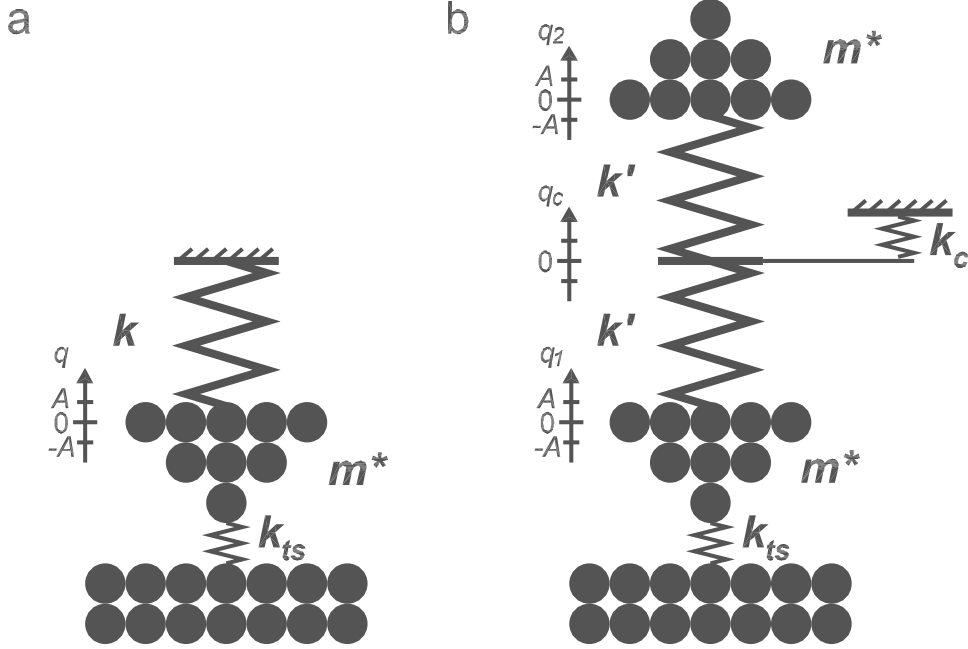


FIG. 3: a) Mechanical analog of a single oscillator-type force sensor (standard cantilever or qPlus sensor as in Fig. 1a), consisting of a single oscillating beam. The single oscillator has only one degree of freedom, its deflection  $q$ . b) Mechanical analog of a coupled oscillator used as a force sensor (tuning fork or length extensional resonator as in Fig 1e). The coupled oscillator has three degrees of freedom: the deflection of the central mount  $q_c$  and the deflections of the two coupled oscillators  $q_{1,2}$ .

## II. FREQUENCY SHIFT AS A FUNCTION OF TIP-SAMPLE INTERACTION FOR SINGLE AND COUPLED OSCILLATORS

In frequency modulation atomic force microscopy, the eigenfrequency  $f$  of a force sensor (such as a qPlus sensor or a needle sensor, see Fig. 2) that vibrates at a constant amplitude  $A$  changes with the action of force gradients by a frequency shift  $\Delta f = f - f_0$ . With  $f = f_0 + \Delta f$  and  $f_0 = \frac{1}{2\pi}\sqrt{k/m^*}$ , the frequency shift is given by

$$\Delta f = \frac{f_0}{2k} \langle k_{ts} \rangle \quad (2)$$

with [27]

$$\langle k_{ts} \rangle(z) = \frac{2}{\pi} \int_{-1}^1 k_{ts}(z + \zeta A) \sqrt{1 - \zeta^2} d\zeta. \quad (3)$$

At large amplitudes, the frequency shift is given by

$$\Delta f = \frac{f_0}{k} \frac{1}{A^{3/2}} \gamma_{ts} \quad (4)$$

with the normalized frequency shift  $\gamma_{ts} \approx 0.4 F_{ts} \sqrt{\lambda}$  [33]. When  $A$  is very small compared to the decay length  $\lambda$  of the force gradient,  $\langle k_{ts} \rangle(z)$  is similar to  $k_{ts}(z)$ , the gradient of the tip-sample forces at the center position of the cantilever that oscillates around  $z \pm A$ .

The eigenfrequency is found by solving the equation of motion for the cantilever deflection  $q(t)$ , the single degree of freedom:

$$m^* \frac{\partial^2 q}{\partial t^2} = -q(k + k_{ts}) \quad (5)$$

resulting in  $q(t) = A \cos(\omega t + \phi)$  with  $\omega^2 = (k + k_{ts})/m^*$  and  $\omega = 2\pi f$ .

Figure 2 b) shows a coupled oscillator such as a tuning fork or a length extensional resonator. In the case of a coupled oscillator, the oscillator has three degrees of freedom  $q_1(t)$ ,  $q_2(t)$  and  $q_c(t)$ , leading to more complicated modes than the case of a cantilever or qPlus sensor with its single degree of freedom. When the inertial forces (given by mass times acceleration) of the center piece of the length extensional resonator can be neglected (a fair assumption for the antiparallel mode), the equation of motion is relatively easy to solve:

$$m^* \frac{\partial^2 q_1}{\partial t^2} = -k_{ts} q_1 + k'(q_c - q_1) \quad (6)$$

$$m^* \frac{\partial^2 q_2}{\partial t^2} = -k'(q_2 - q_c) \quad (7)$$

Because the center of the LER needs to be in equilibrium, we find

$$q_c k_c = k'(q_1 - q_c) + k'(q_2 - q_c) \quad (8)$$

With  $\kappa = 1/(2 + k_c/k')$  we can substitute  $q_c = \kappa(q_1 + q_2)$  and find

$$\frac{\partial^2 q_1}{\partial t^2} = -\omega_0^2 (1 + k_{ts}/k' - \kappa) q_1 + \omega_0^2 \kappa q_2 \quad (9)$$

$$\frac{\partial^2 q_2}{\partial t^2} = +\omega_0^2 \kappa q_1 - \omega_0^2 (1 - \kappa) q_2 \quad (10)$$

with  $\omega_0^2 = k'/m^*$ . Using a harmonic ansatz  $q_{1,2}(t) = A_{1,2} \cos(\omega t + \phi_{1,2})$ , we find two solutions for  $\omega$ :

$$\omega_{1,2}^2 = \omega_0^2 \left\{ 1 - \kappa + \frac{k_{ts}}{2k'} \pm \sqrt{\kappa^2 + \frac{k_{ts}^2}{4k'^2}} \right\}. \quad (11)$$

Typically,  $\kappa < 1/3$  because  $k_c < k'$  and with  $k_{ts} \ll k'$ , we can approximate the square root in eq. 11:

$$\omega_{1,2}^2 \approx \omega_0^2 \left\{ 1 - \kappa + \frac{k_{ts}}{2k'} \pm \kappa \left( 1 + \frac{k_{ts}^2}{8\kappa k'^2} \right) \right\}. \quad (12)$$

Two solutions are found, where the plus sign in eq. 11 corresponds to a high-frequency antiparallel motion ( $A_1 \approx -A_2, \phi_1 = \phi_2$ )

$$\omega_1^2 \approx \omega_0^2 \left\{ 1 + \frac{k_{ts}}{2k'} + \frac{k_{ts}^2}{8k'^2} \right\} \quad (13)$$

and the minus sign to a low frequency parallel motion ( $A_1 \approx A_2, \phi_1 = \phi_2$ )

$$\omega_2^2 \approx \omega_0^2 \left\{ 1 - 2\kappa + \frac{k_{ts}}{2k'} - \frac{k_{ts}^2}{8k'^2} \right\}. \quad (14)$$

The antiparallel motion is used in force microscopy with coupled oscillators, where the frequency shift of the sensor is given by

$$\frac{\omega_1 - \omega_0}{\omega_0} = \frac{\Delta f}{f_0} = \frac{k_{ts}}{4k'} \quad (15)$$

(in leading order of  $k_{ts}$ ). The frequency shift for a coupled oscillator is thus only half the value of the single oscillator after eq. 2. We can still use eqs. 2 and 4 by defining an effective stiffness  $k$  that is twice as large as the individual stiffness  $k'$  of each of the two coupled oscillators.

$$k_{coupled} = 2k'. \quad (16)$$

Equation 2 links the signal (i.e. the physical observable) to  $k_{ts}$ , the physical origin of the signal by multiplying it with the prefactor  $f_0/2k$ . To obtain a strong signal, the prefactor  $f_0/2k$  should be large. For a tip-sample force gradient of 1 N/m, a standard needle sensor would yield a frequency shift of  $\Delta f = 0.463$  Hz, while a standard qPlus sensor would yield a frequency shift of  $\Delta f = 8.33$  Hz. However, to assess the signal-to-noise ratio, we need to consider noise as well as signal strength. Noise also depends on the sensor type and will be discussed in section V.

### III. OPERATING PRINCIPLES AND SENSITIVITY OF QUARTZ SENSORS

#### A. Sensor based on length extensional resonator (needle sensor)

The needle sensor has a very simple operating principle. It consists of two coupled beams that oscillate opposite to each other (see Fig. 1). The longitudinal stiffness of  $k'$  of each of

the two bars that constitute the needle sensor is given by

$$k' = \frac{Ewt}{L}, \quad (17)$$

with Young's modulus  $E$ , length  $L$ , width  $w$  and thickness  $t$  of each quartz beam. The fundamental eigenmode is a longitudinal standing wave with a node at the root of each beam and its end at a maximal deflection, thus the length of one beam  $L$  corresponds to a quarter wavelength  $\lambda/4$ . Because the velocity of sound is  $v_s = \sqrt{E/\rho}$  with mass density  $\rho$ , the eigenfrequency is given by

$$f_0 = \frac{v_s}{4L}. \quad (18)$$

The deflection of a cross section at a distance  $z$  from the mount is given by

$$\delta z(z) = A \sin\left(\frac{\pi z}{2L}\right) \quad (19)$$

when the ends of the device oscillate at amplitude  $A$ . The strain as a function of  $z$ -position is then given by

$$\epsilon(z) = \frac{\partial \delta z(z)}{\partial z} = \frac{\pi A}{2L} \cos\left(\frac{\pi z}{2L}\right). \quad (20)$$

The strain  $\epsilon$  leads to a mechanical stress  $\sigma_{mech}$  given by

$$\sigma_{mech}(z) = E\epsilon(z). \quad (21)$$

The piezoelectric effect causes the emergence of a surface charge density  $\sigma_{el}$  given by

$$\sigma_{el}(z) = d_{21}\sigma_{mech}(z) \quad (22)$$

where  $d_{21} = 2.31 \text{ pC/N}$  is the transverse piezoelectric coupling coefficient of quartz [45], which is equal to the longitudinal piezoelectric coupling coefficient  $d_{11}$ . It is important to note that  $d_{21}$  is essentially constant over the temperature range from 1.5 K to room temperature [45]. When the charge density is integrated over the surface of the sensor, the total charge  $q_{el}$  at a given deflection  $A$  is given by:

$$q_{el} = d_{21}w \int_{-L_e}^{L_e} E \frac{A\pi}{2L} \cos\left(\frac{z\pi}{2L}\right) dz. \quad (23)$$

Thus, the sensitivity is given by

$$S_{LER}^{theory} = q_{el}/A = 2d_{21}Ew \sin\left(\frac{L_e\pi}{2L}\right). \quad (24)$$

With eq. 17, we can express eq. 24

$$S_{LER}^{theory} = 2d_{21}k' \frac{L}{t} \sin\left(\frac{\pi L_e}{2L}\right). \quad (25)$$

The electrodes extend almost to the end of the beams ( $L_e = 1.1$  mm,  $L = 1.34$  mm), therefore, the sine in the equation above is almost one (exact value 0.960685188) and with  $L/t = 1340/70$ , we find  $S_{LER}^{theory} \approx 19 \times d_{21} \times k'$ . With the stiffness  $k' = 540$  kN/m, we find a theoretical sensitivity of  $S_{LER}^{theory} = 45$   $\mu$ C/m.

### B. Sensor based on quartz tuning fork (qPlus sensor)

For a rectangular cantilever with width  $w$ , thickness  $t$  and length  $L$ , the spring constant  $k$  is given by [31]:

$$k = \frac{Ewt^3}{4L^3}. \quad (26)$$

where  $E$  is Young's modulus. The fundamental eigenfrequency  $f_0$  is given by [31]:

$$f_0 = 0.162 \frac{t}{L^2} v_s \quad (27)$$

where  $v_s$  is the speed of sound in quartz as defined above.

The calculation of the sensitivity is slightly more complicated than in the case of the needle sensor. Here, we adapt the result from [15]:

$$S_{qPlus}^{theory} = q_{el}/A = 12d_{21}k \frac{L_e(L - L_e/2)}{t^2}. \quad (28)$$

Standard qPlus sensors with dimensions listed in table I yield  $S_{qPlus}^{theory} = 2.8$   $\mu$ C/m. It is important to note that the calculated sensitivity assumes a field distribution as shown in Fig. 2 e), while the actual field looks more like Fig. 2 c).

## IV. SIGNAL

In FM-AFM, the signal is a frequency shift  $\Delta f$ . This frequency shift depends on the tip sample interaction and the stiffness  $k$ , eigenfrequency  $f_0$  and amplitude  $A$  of the cantilever. For a force that follows an exponential distance dependence  $F(z) = F_0 \exp(-\kappa z)$ , we find

$$\Delta f = \frac{f_0}{kA} F_0 e^{-\kappa(z+A)} I_1(\kappa A) \quad (29)$$

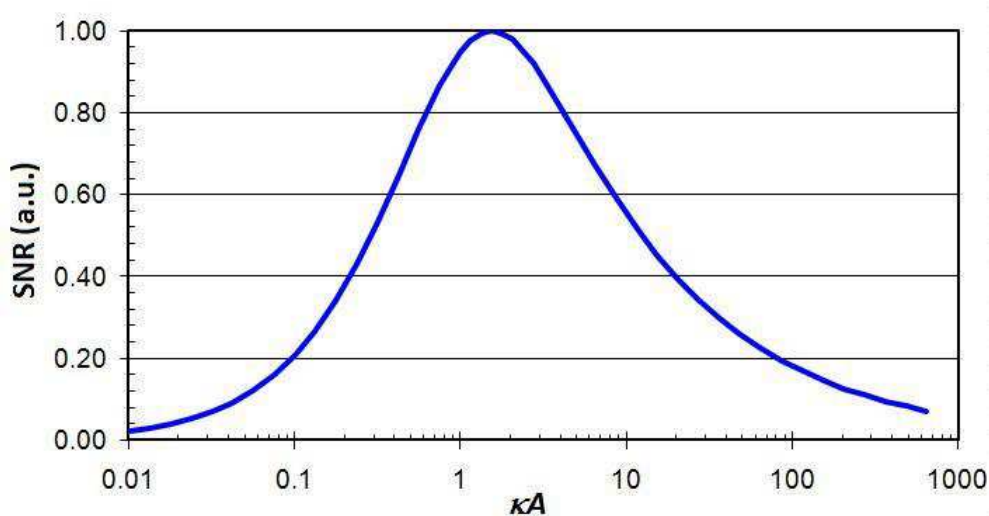


FIG. 4: Signal-to-noise ratio (SNR) as a function of the product between decay constant  $\kappa$  and amplitude  $A$ , where the decay constant  $\kappa$  is inverse to the interaction length  $\lambda$ , thus  $\kappa = 1/\lambda$ . Optimal SNR is obtained for  $\kappa A = A/\lambda = 1.545$ .

where  $I_1(\kappa A)$  is the Bessel function of the first kind, a special version of the Kummer function [33].

As we will see below, the noise in the frequency measurement of the sensor is inversely proportional to  $A$ , therefore the signal-to-noise ratio ( $SNR$ ) can be expressed as

$$SNR \propto e^{-\kappa A} I_1(\kappa A). \quad (30)$$

This function has its maximum at  $\kappa A = 1.5451\dots$ , thus, the optimal signal-to-noise ratio is reached for amplitudes that correspond to the decay length  $\lambda = 1/\kappa$  of the tip-sample force [6], or more precisely  $A_{opt} \approx 1.545\lambda$ . In theory, this ideal amplitude applies to all sensors in FM-AFM that probe interactions of range  $\lambda$ , provided the sensor stiffness is sufficient to enable stable oscillation close to the surface [6].

We can rewrite eq. 29 such that its resemblance to the gradient approximation becomes more clear:

$$\Delta f = \frac{f_0}{2k} \kappa F_0 e^{-\kappa/(z+A)} \frac{2I_1(\kappa A)}{\kappa A} \quad (31)$$

For a minimum distance between tip and sample of  $z$ , the tip oscillates within the interval  $[z..z+2A]$  and at the optimal oscillation amplitude  $A_{opt} \approx 1.545/\kappa$ , we obtain an average tip-

sample force gradient that is approximately one third of the peak force gradient at distance  $z$ , because  $2I_1(1.5451)e^{-1.5451}/1.5451 \approx 0.33$ .

We can now calculate the frequency shift assuming that a single chemical bond is responsible for the contrast. A covalent bond between a Si tip atom and an adatom on Si(111)-(7×7) can be modelled by a Morse Potential

$$V_{Morse} = E_{bond}(-2e^{-\kappa(z-\sigma)} + e^{-2\kappa(z-\sigma)}) \quad (32)$$

with the following fitting parameters: bond strength  $E_{bond} = 2.273$  eV, equilibrium distance  $\sigma = 235.7$  pm and decay constant  $\kappa = 2 \times 1.497 / 0.2357 \text{ nm}^{-1} = 12.70 \text{ nm}^{-1}$  [38]. The optimal amplitude to measure this bond in the attractive regime is therefore  $A_{opt} = 1.545 / 12.7 \text{ nm} = 122$  pm. The repulsive regime of this bond would ideally be probed with an amplitude of 61 pm, because the range of the repulsive force component is only half the range of the attractive component. Figure 5 displays the force gradient and the frequency shifts corresponding to a sensor that oscillates in a force field given by this Morse potential.

Figure 5 shows that at the optimal oscillation amplitude, a minimal frequency shift of -70 Hz can be expected for a standard qPlus sensor and -3.5 Hz for a standard needle sensor when probing a single silicon bond. However, on weakly bonding systems such as organic molecules, frequency shifts on the order of -5 Hz for a qPlus sensor [23], corresponding to -250 mHz for a needle sensor may result.

## V. NOISE

If the frequency of the force sensor could be measured with infinite accuracy, infinitely small force gradients could be measured. In practice, there are four relevant noise contributions that need to be considered. For large bandwidths, i.e. for large scanning speeds, deflection detector noise is dominant. deflection detector noise increases with  $B^{3/2}$ . Two other noise sources, thermal noise and oscillator noise, increase with the square root of bandwidth  $B$ . The fourth noise source is due to sensor frequency drifts caused by temperature changes. Thermal frequency drift is a challenge for room temperature measurements and in particular for high-temperature measurements. Because we measure an average force gradient in FM-AFM, the noise in this figure is given with eq. 2

$$\delta k_{ts} = 2k \frac{\delta f}{f_0}. \quad (33)$$

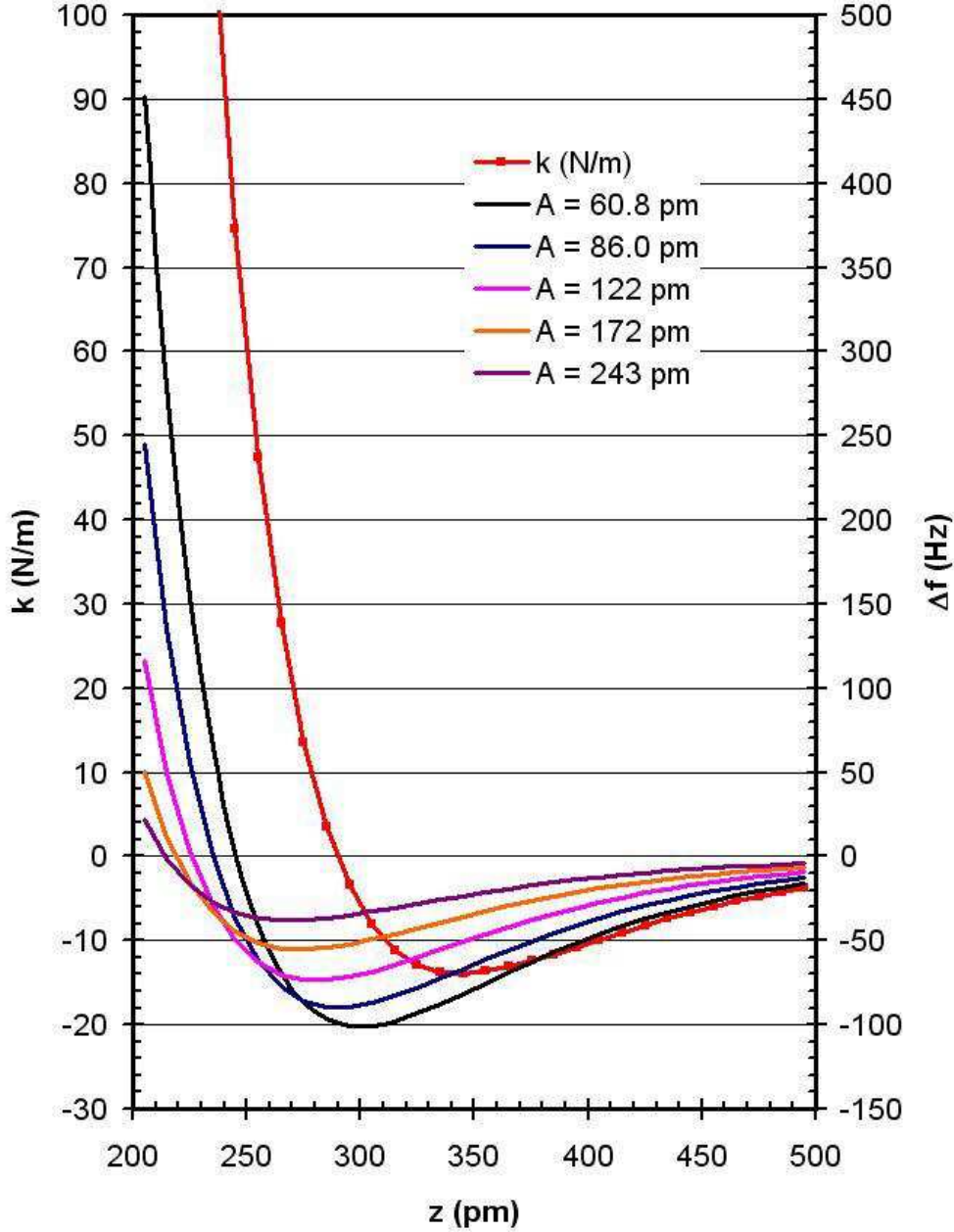


FIG. 5: Force gradient (red) and calculated frequency shift for the interaction of a silicon tip with an adatom on Si(111)-(7×7) surface modelled by a Morse potential with  $E_{bond} = 2.273$  eV,  $\sigma = 235.7$  pm and  $\kappa = 12.70$  nm<sup>-1</sup> for a qPlus sensor with  $k = 1800$  N/m and  $f_0 = 30$  kHz and various amplitudes (see legend). If a standard needle sensor was used here, the frequency shift values denoted on the right vertical axis have to be multiplied by 1/20, because the frequency shift is proportional to  $f_0/k$ . For the qPlus sensor, a minimal frequency shift of -70 Hz results at the optimal amplitude  $A = 122$  pm, while the needle sensor only yields a minimal frequency shift of -3.5 Hz.

### A. Deflection sensor noise

The deflection of the cantilever can not be measured with infinite precision, but is subject to noise. Typically, the oscillation frequency of the cantilever varies very little around the eigenfrequency  $f_0$  and we can therefore assume a constant deflection detector noise density  $n_q$  that denotes the precision at which the deflection of the cantilever can be measured (e.g. for  $n_q = 100 \text{ fm}/\sqrt{\text{Hz}}$ , the error in deflection measurement is  $\delta q = 100 \text{ fm}$  at a bandwidth of 1 Hz and  $\delta q = 1 \text{ pm}$  at a bandwidth of 100 Hz). This uncertainty in the deflection measurement also leads to frequency noise [34–36], given by

$$\frac{\delta f_{\text{sensor}}}{f_0} = \sqrt{\frac{2}{3}} \frac{n_q B^{3/2}}{A f_0}. \quad (34)$$

With eq. 33, we find

$$\delta k_{ts \text{ sensor}} = \sqrt{\frac{8}{3}} \frac{k n_q B^{3/2}}{f_0 A}. \quad (35)$$

For quartz sensors, the deflection noise depends on the charge that is generated per deflection and the gain and noise of the preamplifier. Current-to-voltage converters convert the current provided by the quartz sensor to a voltage. However, the frequency response of the current-to-voltage converter is not independent of frequency, but given by

$$V_{\text{out}} = -\frac{RI}{1 + i2\pi fRC}, \quad (36)$$

where  $R$  is the resistance of the feedback resistor and  $C$  is its parasitic capacitance. The solid line in figure 7 shows the theoretical frequency response of an ideal operational amplifier with  $R = 100 \text{ M}\Omega$  and a parasitic capacitance of  $C = 0.2 \text{ pF}$ . The gain is flat for frequencies smaller than the corner frequency  $f_{c1} = 1/(2\pi RC) = 7.96 \text{ kHz}$ . For  $f \gg f_{c1}$ , the gain is given by  $V_{\text{out}} = -I/(i2\pi fC)$  - inversely proportional to  $f$ . A sinusoidally varying charge  $Q_{ch} = Q_0 \exp(i2\pi ft)$  corresponds to a current  $I = \dot{Q}_{ch} = Q_0 i2\pi f \exp(i2\pi ft)$ , thus the gain can be expressed as  $V_{\text{out}} = -Q_{ch}/C$ . Therefore, this amplifier is called a ‘charge amplifier’ for frequencies significantly larger than  $f_{c1}$ . Simple amplifiers as the one shown in Fig. 6 often display a second corner frequency  $f_{c2}$  not very much higher than  $f_{c1}$  and for frequencies beyond  $f_{c2}$  the gain decays proportional to  $1/f^2$ . The charge amplifier that is used here for the needle sensor [40] has an  $f_{c2}$  at around 15 MHz and is therefore suited well for high-frequency sensors. The question is now, when is it advisable to use a current-to-voltage converter, and when is it favorable to use a charge amplifier. Figure 7 shows that

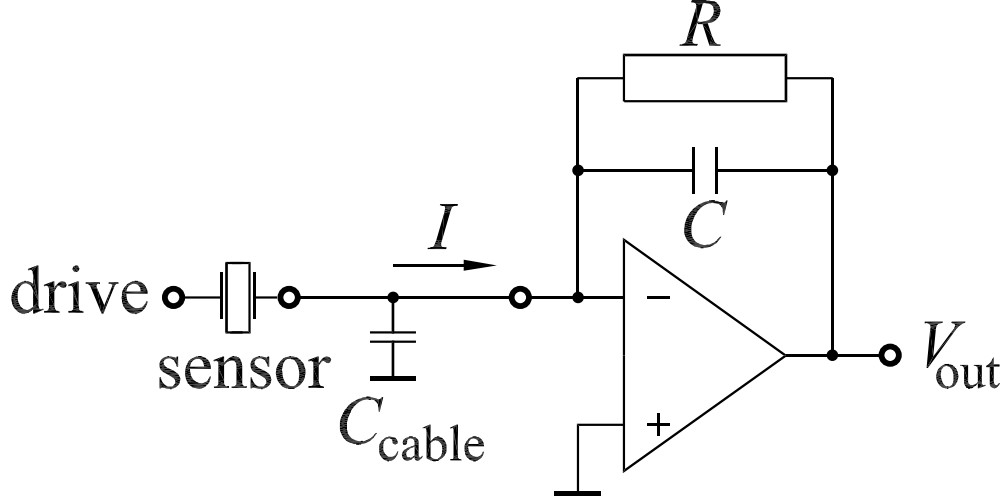


FIG. 6: Schematic of a quartz sensor, cable and current-to-voltage converter that is often used for amplifying deflection data from quartz sensors. The gain of the amplifier is given by  $V_{out} = -RI/(1 + if/f_{c1})$  with its first corner frequency  $f_{c1}$  given by  $f_{c1} = 1/(2\pi RC)$ . The capacity of the cable should be as low as possible - cable capacity increases noise in the amplifiers output. If the amplifier is vacuum compatible, it can be placed close to the sensor, thus reducing cable capacity and noise. The sensor can be excited electrically as shown in this figure or mechanically - the drive signal is grounded in this case.

the current-to-voltage converter becomes a charge amplifier for sufficiently large frequencies. While one can increase  $f_{c1}$  by reducing the value of the feedback resistor  $R$ , a reduction of  $R$  increases the current noise. The tradeoff between noise and bandwidth leads to an optimal amplifier type for a given operating frequency. Here, we found out that our home-built current-to-voltage converter has a better signal-to-noise ratio for frequencies around  $80 \pm 20$  kHz, while the FEMTO amplifier [40] works better for frequencies above [47]. For charge amplifiers, the deflection detector noise density can be expressed by

$$n_q = \frac{n_{amp}}{S} \quad (37)$$

where  $n_{amp}$  is the noise density of the preamplifier and  $S$  is the sensitivity (charge per deflection) as calculated for the needle sensor in eq. 25 and for the qPlus sensor in eq. 28.

$$\delta k_{ts\ sensor} = \sqrt{\frac{8}{3}} \frac{k}{S f_0} n_{amp} \frac{B^{3/2}}{A}. \quad (38)$$

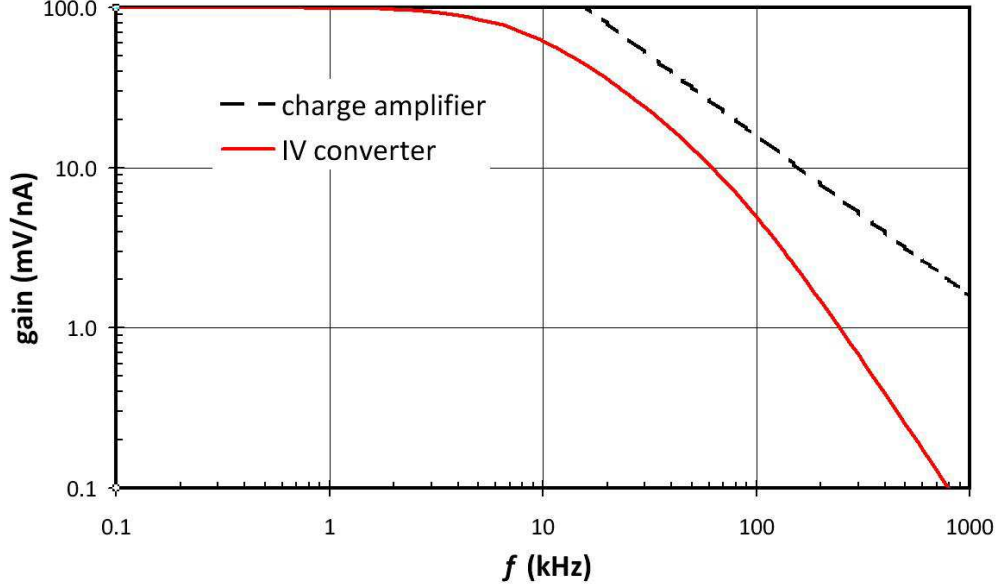


FIG. 7: Current gain versus frequency for a current-to-voltage converter built from an ideal operational amplifier and a  $100\text{ M}\Omega$  feedback resistor with a parasitic capacitance of  $0.2\text{ pF}$  (solid line), yielding a first corner frequency (here,  $f_{c1} = 8\text{ kHz}$ ). For frequencies higher than  $f_{c1}$ , the gain drops proportional to  $1/f$ . Typically, these simple amplifiers develop a second corner frequency (here  $f_{c2} = 80\text{ kHz}$ ) [47], for frequencies higher than  $f_{c2}$ , their gain drops proportional to  $1/f^2$ . The dashed line displays the gain of a commercial charge amplifier [40] with a constant gain of  $10^{13}\text{ V/C}$  (dashed line) for a remarkably large frequency range from  $250\text{ Hz}$  to  $15\text{ MHz}$ .

This equation shows, that the deflection detector noise is small for small spring constants, small amplifier noise, large sensitivity and large eigenfrequency. Thus, the figure of merit for the sensor is not  $S$  alone, but  $Sf_0/k$ . For both needle and qPlus sensors, the sensitivity is proportional to  $k$ . We find for the needle sensor

$$\delta k_{ts\text{needle sensor}} = \sqrt{\frac{8}{3} \frac{n_{amp} t B^{3/2}}{d_{21} L A f_0}} \quad (39)$$

for the ideal case of  $L_e = L$ . For the qPlus sensor, we find

$$\delta k_{ts\text{qPlus sensor}} = \sqrt{\frac{8}{3} \frac{n_{amp} t^2 B^{3/2}}{6 d_{21} L^2 A f_0}}, \quad (40)$$

again assuming the ideal case of  $L_e = L$ . Thus, deflection detector noise depends on the properties of the sensor and the amplifier. If we assume a charge noise density of  $n_{amp} = 90\text{ zC}/\sqrt{\text{Hz}}$  (such as achieved by the commercial FEMTO amplifier [40] when loaded with

a 1 m coaxial cable corresponding to a 100 pF cable capacitance), we can now calculate an explicit number for the deflection detector noise contribution to the force gradient noise with  $A = 100$  pm and the geometrical values after table I. For the needle sensor, we find a theoretical deflection detector noise contribution of

$$\delta k_{ts\ needle\ sensor} = 33.2 \mu\text{N/m} \frac{B^{3/2}}{\text{Hz}^{3/2}} \quad (41)$$

and for the qPlus sensor, we find a theoretical deflection detector noise contribution of

$$\delta k_{ts\ qPlus\ sensor} = 25.7 \mu\text{N/m} \frac{B^{3/2}}{\text{Hz}^{3/2}} \quad (42)$$

For a bandwidth of 100 Hz, the theoretical deflection detector noise contribution is thus 33.2 mN/m for the needle sensor and 25.7 mN/m for the qPlus sensor. However, we have based this calculation on the theoretical sensitivity of the sensors, we will see further below that while the experimental sensitivity of the needle sensor matches theory, the qPlus sensor develops only about 50 % of the theoretical sensitivity. deflection detector noise depends dramatically on bandwidth, it can be reduced substantially by bandwidth reduction. At low temperatures, where slow scanning is possible, the bandwidth can be reduced to one Hertz or less and tiny force gradients can be detected in this case. For a bandwidth of 1 Hz, the deflection detector noise contribution is thus 33.2  $\mu\text{N/m}$  for the needle sensor and 25.7  $\mu\text{N/m}$  for the qPlus sensor. However, at low bandwidth the remaining three noise sources are typically much larger than deflection noise.

## B. Thermal noise

The thermal noise of a force sensor at a bandwidth  $B$  is given by [2]:

$$\frac{\delta f_{thermal}}{f_0} = \sqrt{\frac{k_B T B}{\pi k A^2 f_0 Q}}. \quad (43)$$

Thus, the thermal noise in force gradient measurement is given by

$$\delta k_{ts\ thermal} = \sqrt{\frac{4k k_B T B}{\pi A^2 f_0 Q}} \propto \sqrt{\frac{k}{f_0 Q}}. \quad (44)$$

For the needle sensor, reasonable  $Q$  values are 15 000 at room temperature and 50 000 at 4 K. For the qPlus sensor,  $Q \approx 3$  000 at room temperature, reaching up to 200 000 at 4 K [39]. Thus, at room temperature the thermal contribution to the minimal detectable force

gradient is  $\delta k_{ts\,thermal} = 6 \text{ mN/m per } \sqrt{\text{Hz}}$  for the needle sensor and  $\delta k_{ts\,thermal} = 3 \text{ mN/m per } \sqrt{\text{Hz}}$  for the qPlus sensor. At  $T = 4 \text{ K}$ , the minimal detectable force gradient is  $\delta k_{ts\,thermal} = 390 \mu\text{N/m per } \sqrt{\text{Hz}}$  for the needle sensor and  $\delta k_{ts\,thermal} = 40 \mu\text{N/m per } \sqrt{\text{Hz}}$  for the qPlus sensor. Again, these calculations refer to  $A = 100 \text{ pm}$ .

### C. Oscillator noise

Recently, Kobayashi et al. [35] discovered a new contribution to frequency noise in FM-AFM that arises in particular in low  $Q$  environments. However, this contribution is not explicitly temperature dependent and thus can become significant at low temperatures where thermal noise becomes small. The origin of this noise can be understood as a driving of the cantilever off resonance because the amplitude feedback is fed with a noisy input signal (due to a finite  $n_q$ ). The lower the  $Q$ -value, the more of this noise pushes the cantilever at the correct phase, therefore, this noise contribution is proportional to  $n_q$  and inversely proportional to  $Q$ :

$$\frac{\delta f_{osc}}{f_0} = \frac{n_q B^{1/2}}{\sqrt{2}AQ}. \quad (45)$$

With eq. 33, we find

$$\delta k_{ts\,osc} = \sqrt{2} \frac{kn_q}{Q} \frac{B^{1/2}}{A}. \quad (46)$$

Similar to thermal noise, oscillator noise is proportional to the square root of the detection bandwidth  $B$  and inversely proportional to amplitude. For the  $Q$  values from above, we find room temperature values of  $\delta k_{ts\,osc} = 4.6 \text{ mN/m per } \sqrt{\text{Hz}}$  for the needle sensor and  $\delta k_{ts\,thermal} = 0.6 \text{ mN/m per } \sqrt{\text{Hz}}$  for the qPlus sensor. At  $T = 4 \text{ K}$ , the contribution of oscillator noise to the minimal detectable force gradient is  $\delta k_{ts\,osc} = 1.4 \text{ mN/m per } \sqrt{\text{Hz}}$  for the needle sensor and  $\delta k_{ts\,thermal} = 9.5 \mu\text{N/m per } \sqrt{\text{Hz}}$  for the qPlus sensor. Again, these calculations refer to  $A = 100 \text{ pm}$ .

### D. Thermal frequency drift noise

Temperature variations cause a drift in eigenfrequency. For silicon cantilevers, the relative frequency variation is linear with temperature with a value of  $-35 \text{ ppm/K}$  at room temperature [8]. Thus, a hypothetical Si cantilever with  $k = 1 \text{ kN/m}$  (this large stiffness would be required to enable stable oscillation at small amplitudes) would be subject to

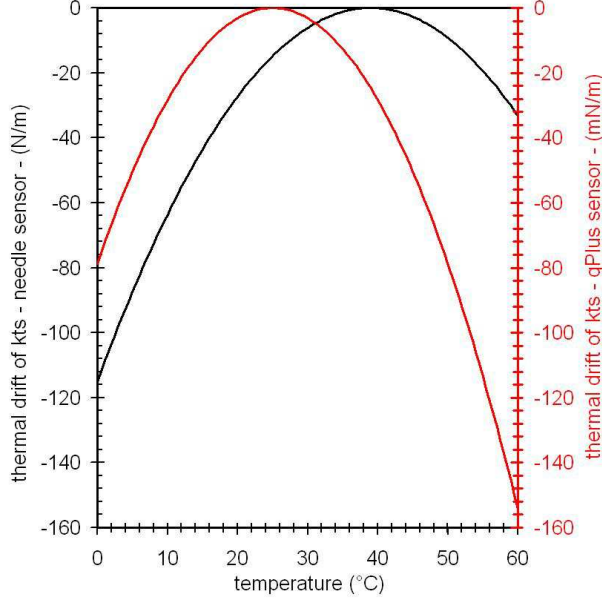


FIG. 8: Effect of temperature changes on the measured tip-sample force gradient. Both needle sensor and qPlus sensor change their frequency as a function of temperature. Although the relative frequency shift is much smaller than for silicon cantilevers, the effect on the measured force gradient scales with stiffness  $k$ . This thermal frequency drift noise is almost three orders of magnitude smaller for the qPlus sensor than for the needle sensor.

a  $\langle k_{ts} \rangle$  drift of  $-35 \text{ mN/m/K}$ . Quartz sensors show a quadratic frequency shift with temperature and the eigenfrequency varies with temperature as an inverted parabola centered around the *turnover temperature*  $T_p$ [43]:

$$\frac{\delta f_{sensor}}{f_0} = -\chi(T - T_p)^2. \quad (47)$$

The turnover frequency depends on the crystal cut (see Fig. 9 in [37]). Tuning fork crystals are often cut to yield  $T_p = 298 \text{ K}$  such that the turnover temperature is close to the temperature that a watch that is strapped to a wrist typically develops. Length-extensional-resonators, in contrast, are often oriented such that their turnover temperature is around  $313 \text{ K}$  [43], probably because  $1 \text{ MHz}$  crystals are typically not worn on the wrist but built into printed circuit boards that have higher operating temperatures than the human body. This thermal frequency drift causes a thermal drift in force gradient measurement given by

$$\delta k_{ts\ drift} = -2k\chi(T - T_p)^2. \quad (48)$$

Although the temperature stability of quartz is excellent with very small values of  $\chi = 35 \times 10^{-9} \text{K}^{-2}$ , the net effect on the precision on the measurement of  $\langle k_{ts} \rangle$  is proportional to the effective stiffness of the sensor  $k$ .

The quadratic dependence of the frequency variation with temperature is only valid for temperatures around  $T_p$ . For the temperature range from 300 K to 4 K, the frequency variation has been measured by Hembacher et al. [20] and is approximately given by

$$\frac{\delta f_{sensor}}{f_0} \approx -0.00081[1 - \cos((T/T_p - 1)\pi)] \quad (49)$$

with a total relative frequency change of  $-1620$  ppm over the temperature range from 300 K to 4 K. An et al. have found a similar frequency change of a needle sensor (Fig.3 in [29]) from 998066 Hz at 300 K to 996314 Hz, corresponding to  $-1755$  ppm. This equation shows that frequency drift with temperature is particularly large for temperatures between room temperature and absolute zero. However, while this approximate formula models the data measured by Hembacher et al. [20] quite precise down to liquid helium temperatures, a detailed measurement of the eigenfrequency of a qPlus sensor has shown that the frequency shows a minimum around 23 K and an increase as the temperature decreases to 4 K at a rate of approximately  $-7.5$  ppm/K at 4 K. Figure 9 shows the dependence of the relative frequency shift for low temperatures. Because the relative frequency shift is mainly dependent on the variation of the velocity of sound with temperature (pp. 38 in [48]), we expect a similar relative frequency shift for the qPlus sensor and the needle sensor also in the temperature range from 4 K to 30 K. To obtain the variation in the measured tip-sample force gradient  $\langle k_{ts} \rangle$ , the relative frequency shift has to be multiplied by  $2k$ . For the qPlus sensor, we obtain a  $\langle k_{ts} \rangle$  drift of  $-27 \mu\text{N/m}$  per milliKelvin and for the needle sensor, we get  $-16 \text{mN/m}$  per milliKelvin. Because variations in ambient pressure cause a slight change in boiling temperature of the helium bath, we expect that temperature drift can become a significant issue for the needle sensor even at low temperature.

### E. Summary of noise calculations

In summary, we find that the large spring constant of the needle sensor is not a significant disadvantage regarding deflection sensor noise, because although the frequency shift that a sensor is subject to is proportional to  $1/k$ , the sensitivity is proportional to  $k$ , and the two

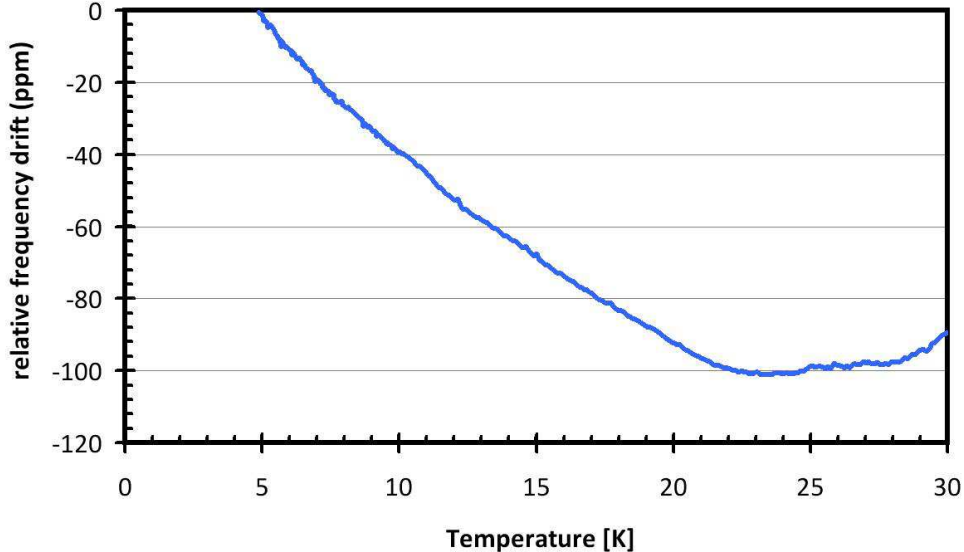


FIG. 9: Relative frequency shift of a qPlus sensor at low temperatures. The minimal frequency does not occur at absolute zero, but approximately at 23 K. At a temperature of 4 K, the relative frequency drift is -7.5 ppm/K.

effects cancel. However,  $k$  does affect the other three noise sources: thermal noise increases as  $\sqrt{k}$ , and both oscillator noise and frequency drift noise are proportional to  $k$ . Therefore, the recommendations in eq. 1, stating that  $k$  should be large enough to enable stable sensor oscillations at the optimal amplitude but otherwise as small as possible are still valid. High  $Q$ -values are desirable to minimize thermal and oscillator noise. The frequency drift noise can be minimized by operating the sensors in a thermally stable environment, preferentially at temperatures at or close to  $T_p$ .

## VI. EXPERIMENTAL NOISE MEASUREMENTS

So far, we have only considered theoretical calculations to compare the noise characteristics of the two sensors studied here. Now, we supplement the calculations by measurements. First, we measure the thermal noise peak of the needle sensor and the qPlus sensor with sensors of standard dimensions listed in table I. The equipartion theorem states, that an oscillator carries a thermal energy  $k_B T/2$  per degree of freedom, where  $k_B$  is Boltzmann's constant and  $T$  is the temperature in Kelvin. For the standard qPlus sensor, we find the thermal am-

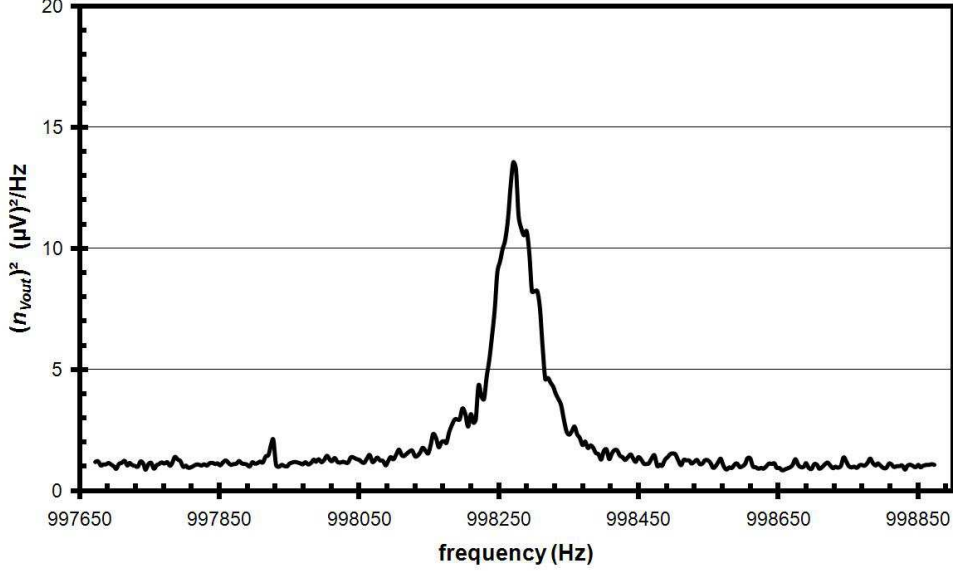


FIG. 10: Thermal spectrum of a needle sensor with standard dimensions at room temperature and ambient pressure. A commercial preamplifier [40] was used. The sensitivity of the sensor is calculated to  $45.4 \mu\text{C}/\text{m}$ , the  $Q$ -factor is 18500 and the deflection detector noise density is  $1.89 \text{ fm}/\sqrt{\text{Hz}}$ .

plitude by equating the average potential energy to the thermal energy  $kA_{rms}^2/2 = k_B T/2$ , yielding a thermal rms-amplitude of  $A_{rms} = 1.52 \text{ pm}$  or peak- amplitude of  $A_{0p} = 2.14 \text{ pm}$ . For the needle sensor, we need to take into account that it is a coupled oscillator, therefore  $2 \times k' A_{rms}^2/2 = k_B T/2$ , yielding a thermal rms-amplitude of  $A_{rms} = 62 \text{ fm}$  or peak- amplitude of  $A_{0p} = 88 \text{ fm}$ . Figure 10 shows the thermal peak of a needle sensor without tip in ambient conditions. The power spectral density in Fig. 10 was recorded by connecting the output of the FEMTO amplifier [40] to the input of the oscillation controller (OC4 from Nanonis [42]) using the Zoom-FFT (Fast Fourier Transform) feature and correcting the filter error by comparing the output with a dedicated FFT Analyzer at low frequencies (Agilent 35670A Dynamical Analyzer). The input of the femto amplifier was connected to a length extensional resonator (no tip attached) with dimensions given by table I with a coaxial cable with a length of 1 m (capacity approx. 100 pF). The commercial preamplifier has a noise density of  $n_{amp} = 90 \text{ zC}/\sqrt{\text{Hz}}$  when loaded with a 1 m coaxial cable (100 pF cable capacitance) [40] and  $n_{amp} = 40 \text{ zC}/\sqrt{\text{Hz}}$  without cable (sensor directly connected to the amplifier) at the operating frequency of the needle sensor (1 MHz). From figure 10, we

can calculate the sensitivity as well as the deflection detector noise density by following the procedure published in [15].

For the needle sensor, we find an experimental sensitivity of  $S = 45.4\mu\text{C}/\text{m}$ , that is 100% of the theoretical value. In a previous measurement, the needle sensor reached only 44% of the theoretical value [28]. A possible reason for a deviation between theoretical and experimental sensitivity in the previous measurement might be attributed to cable capacity between sensor and amplifier and non-ideal amplifier performance. The deflection detector noise density is thus  $n_q = 2\text{ fm}/\sqrt{\text{Hz}}$  with a 1 m cable and  $n_q = 0.89\text{ fm}/\sqrt{\text{Hz}}$  when the sensor is directly connected to the preamp (not feasible for vacuum operation).

At 30 kHz, the operating frequency of the qPlus sensor, we measured  $n_{amp} = 122\text{ zC}/\sqrt{\text{Hz}}$  with a 1 m coaxial cable (100 pF cable capacitance) for the FEMTO amplifier [40] and  $n_{amp} = 86\text{ zC}/\sqrt{\text{Hz}}$  without cable. Thus, a standard qPlus sensor would yield  $n_q = 122\text{ zC}/\sqrt{\text{Hz}}/1.44\mu\text{C}/\text{m} = 85\text{ fm}/\sqrt{\text{Hz}}$ . When directly connected to the amplifier, the qPlus sensor would achieve a deflection detector noise density of  $n_q = 62\text{ fm}/\sqrt{\text{Hz}}$  at room temperature. The homebuilt amplifier can be cooled, and its noise at 4 K typically drops to 50% [20], yielding  $n_q = 31\text{ fm}/\sqrt{\text{Hz}}$  at 4 K. Using our home-built amplifier for the qPlus sensor, we obtain a deflection detector noise density of  $n_q = 62\text{ fm}/\sqrt{\text{Hz}}$ . The home-built amplifier is vacuum and UHV compatible and therefore can be connected closely to the sensor, thereby greatly reducing  $C_{cable}$ . The power spectral density in Fig. 10 was recorded by connecting the output of a home-built UHV compatible amplifier to the input of the Nanonis OC4 PLL and recording its FFT (Fast Fourier Transform) output. The input of the amplifier was connected to a qPlus sensor without tip with dimensions given by table I with a short cable with a length of approx. 0.1 m (capacity approx. 10 pF). The experimental result is  $S_{qPlus}^{exp} = 1.44\mu\text{C}/\text{m}$  - about 51 % of the theoretical value. The deviation between the theoretical and experimental values is probably due to edge effects - the calculation of the sensitivity is based on a homogenous field distribution and an electrode configuration in the quartz crystal as in Fig. 2 e, while the actual field distribution is perturbed by edge effects as in Fig. 2 c. For the needle sensor, the deviation between actual (Fig. 2 h) and ideal field (Fig. 2 j) is much smaller, therefore its experimental sensitivity is essentially equal to the calculated sensitivity.

Figure 12 shows the calculated (smooth lines) and experimental (jagged lines) power spectral density of the force gradient noise  $n_{kts}$  as a function of modulation frequency  $f_{mod}$ .

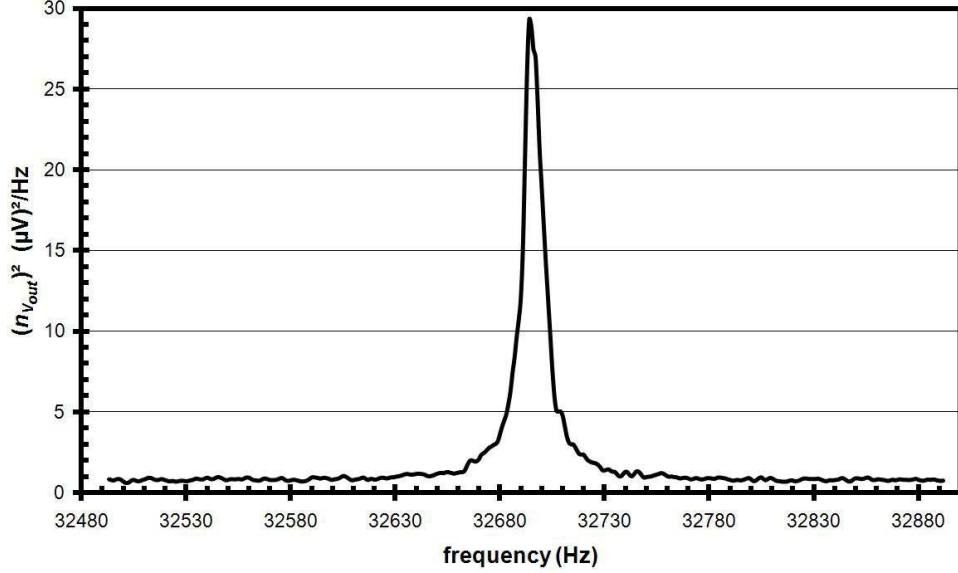


FIG. 11: Thermal spectrum of a qPlus sensor with standard dimensions at room temperature and ambient pressure. A homebuilt preamplifier was used. The sensitivity of the sensor is calculated to  $1.44 \mu\text{C}/\text{m}$ , the  $Q$ -factor is 2900 and the deflection detector noise density is  $62 \text{ fm}/\sqrt{\text{Hz}}$ .

This graph is produced by inserting the output of the phase-locked-loop detector to a FFT Analyzer (Agilent) and multiplying the frequency shift by the corresponding scaling factor ( $k_{ts} = 2k/f_0 \times \Delta f$ , thus  $n_{kts} = 2k/f_0 \times n_{\Delta f}$ ). The total noise of the force gradient measurement is given by

$$\delta k_{ts} = \sqrt{\int_0^B n_{kts}^2(f_{mod}) df_{mod}} \quad (50)$$

The calculated graphs include deflection detector noise (linear with  $f_{mod}$ ), thermal noise (constant with  $f_{mod}$ ) and oscillator noise (also constant with  $f_{mod}$ ). Frequency drift noise, which is large for long measuring times (i.e. small  $f_{mod}$ ) is not included in the calculation, but clearly apparent in the measurement by the increase of the experimental needle deflection detector noise density for small  $f_{mod}$ . The increase of noise for small  $f_{mod}$  in the needle sensor data is related to the strong influence of thermal frequency drift. A random walk in temperature would lead to a random walk in frequency, the Fourier transform of a random walk function leads to a  $1/f$  power distribution [49] As expected, the qPlus sensor shows less thermal, oscillator and frequency drift noise, but slightly more sensor noise. This is due to the excellent adaption of the FEMTO amplifier to the needle sensor and to the fact, that the standard qPlus sensor as described in Table I only has 50% of the calculated sensitivity.

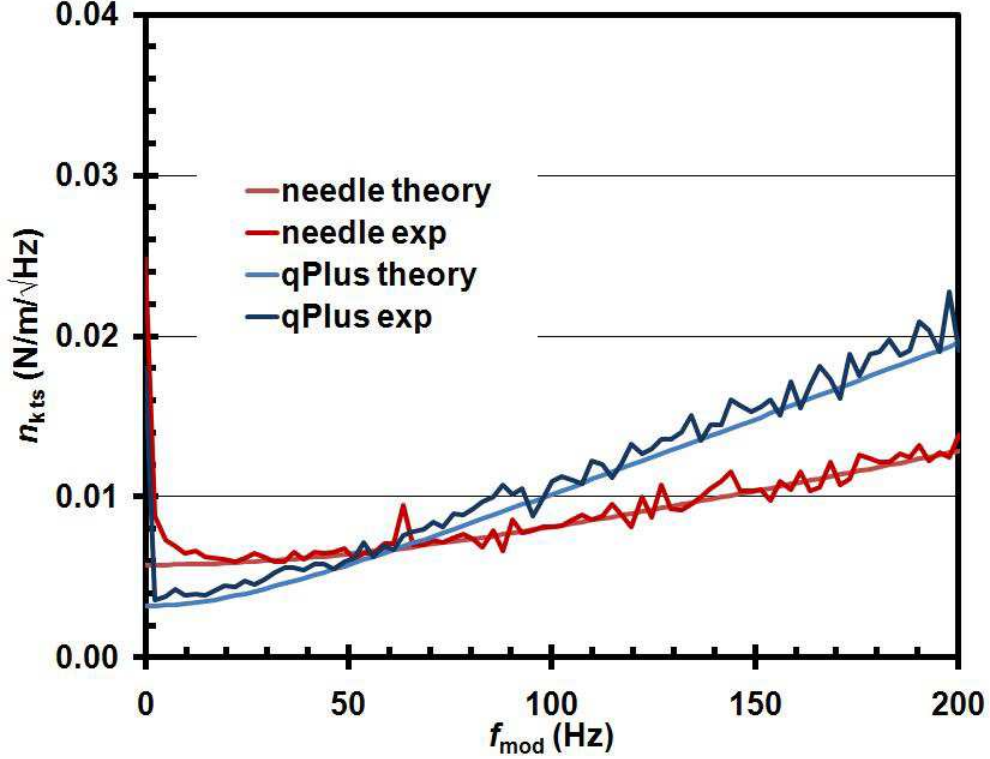


FIG. 12: Total experimental and calculated force-gradient-noise-densities as a function of modulation frequency for the needle sensor (red line) and qPlus sensor (black line) at room temperature. The calculated force force-gradient-noise-densities are derived with the experimental values for  $S, k, n_{amp}, Q$  and  $f_0$  at an amplitude of  $A = 100$  pm.

Table II summarizes the results in a way that all noise contributions can be identified.

## VII. SUGGESTIONS FOR IMPROVEMENTS ON QPLUS AND LER SENSORS

### A. Decreasing deflection sensor noise

With the equations that link signal and noise to the physical parameters of the sensors, we can now attempt to tailor the design values for optimal performance. Equation 40 connects the relative frequency noise (detector contribution) to the sensitivity of the sensor and the

sensor	$n_q$ fm/ $\sqrt{\text{Hz}}$	$Q$	$\delta k_{ts\ det}$ $\frac{\mu\text{N}}{\text{m}}/\text{Hz}^{3/2}$	$\delta k_{ts\ th}$ $\frac{\mu\text{N}}{\text{m}}/\text{Hz}^{1/2}$	$\delta k_{ts\ osc}$ $\frac{\mu\text{N}}{\text{m}}/\text{Hz}^{1/2}$	$\delta k_{ts\ drift}$ $\frac{\text{mN}}{\text{m}}$ at $\Delta T = 0.1\text{ K}$	$\delta k_{ts\ drift}$ $\frac{\text{N}}{\text{m}}$ at $\Delta T = 1\text{ K}$
qPlus 300 K air	62	2900	105	3300	544	0.00126	0.000126
qPlus 300 K UHV	62	15000	105	1450	105	0.00126	0.000126
qPlus 4 K UHV	31	200000	52.6	398	4	-2.7	-0.027
needle 300 K air	1.89	18500	57.7	5550	1560	0.756	0.0756
needle 300 K UHV	1.89	27000	57.7	4590	1070	0.756	0.0756
needle 4 K UHV	1.89	50000	57.7	3370	577	-1620	-16.2

TABLE II: Noise contributions of the four noise sources for qPlus and needle sensor. For both sensors, the  $\delta k_{ts\ drift}$  data are based on Fig. 9.

noise performance of the amplifier. For both sensors, we find

$$\delta k_{ts\ sens} = 2k\sqrt{\frac{2}{3}} \frac{n_{amp}}{SAf_0} B^{3/2}. \quad (51)$$

With eqs. 17, 18 and 25 in the ideal situation of  $L_e = L$ , we can express the spring constant  $k$ , sensitivity  $S$  and eigenfrequency  $f_0$  in terms of the geometrical parameters  $t, w$  and  $L$ :

$$\delta k_{ts\ sens\ ns} = 8\sqrt{\frac{2}{3}} \frac{n_{amp}t}{d_{21}Av_s} B^{3/2}. \quad (52)$$

For the qPlus sensor, we use eqs. 26, 27 and 28 assuming again  $L_e = L$ , finding

$$\delta k_{ts\ sens\ qP} = 1.03\sqrt{\frac{2}{3}} \frac{n_{amp}t}{d_{21}Av_s} B^{3/2}. \quad (53)$$

This result seems quite surprising: deflection detector noise only depends on the thickness  $t$  of the sensor - all the other geometrical dimensions cancel, and when comparing a qPlus and a needle sensor with the same thickness, the qPlus sensor should only display about 1/8 of the noise of the needle sensor if the charge noise of the amplifier in use is similar. If we take into account, that the quartz-cantilever geometry only produces about 50% of the theoretical sensitivity, a qPlus sensor with the same thickness of a needle sensor should display only 1/4 the noise. Miniaturisation therefore appears to be the road to success. The reason for the superior signal-to-noise ratio of the qPlus geometry over the needle geometry lies in the fact that the cross section of the qPlus sensor beam shows a strain and stress profile that is zero in the center and increases towards the edges, where the charge-collecting

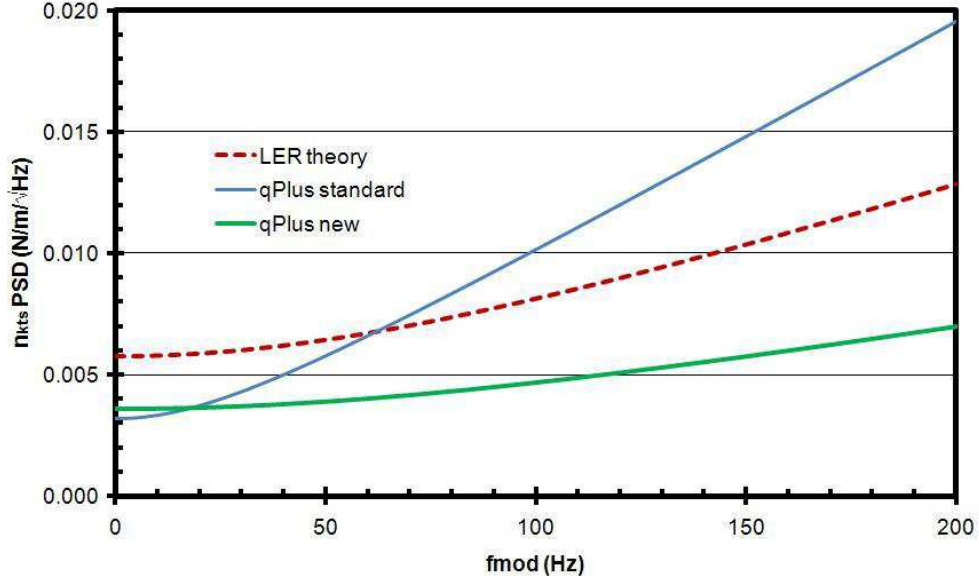


FIG. 13: Calculated force-gradient-noise-densities  $n_{kts}$  as a function of modulation frequency for the standard needle sensor (red line), qPlus sensor (blue line) and a modified qPlus sensor with  $f_0 = 92.8$  kHz,  $k = 3500$  N/m,  $Q = 1650$  and  $n_q = 28$  fm/ $\sqrt{\text{Hz}}$  (green line). The calculated values for  $n_{kts}$  are based on measured values of  $n_{amp}$ ,  $S$ ,  $k$ ,  $f_0$  and  $Q$ .

electrodes are located, while the cross section of the needle sensor has a uniform stress and strain profile (see Fig. 2 d, h). Figure 13 displays the noise figures of standard needle and qPlus sensors and a modified qPlus sensor with a smaller thickness  $t$  and smaller length  $L$  with  $f_0 = 92.8$  kHz,  $k = 3500$  N/m,  $Q = 1650$  and  $n_q = 28$  fm/ $\sqrt{\text{Hz}}$ . This sensor is not only superior to the needle sensor in thermal, oscillator and frequency drift noise, but also in sensor noise.

## B. Decreasing thermal noise

As outlined in equation 44, the thermal noise in the force gradient measurement is given by

$$\delta k_{ts \text{ thermal}}(z) = \sqrt{\frac{4kk_BTB}{\pi A^2 f_0 Q}}, \quad (54)$$

Thus, thermal noise can be minimized by a reduction of temperature, using a stiffness  $k$  as small as possible compatible with stability and choosing a high eigenfrequency  $f_0$  while maintaining a high  $Q$ -value.

### C. Decreasing oscillator noise

Oscillator noise can be minimized by combining the recipes to reduce deflection detector noise and thermal noise, because oscillator noise goes down with decreasing deflection detector noise, increasing  $Q$ , and minimizing  $k$ .

### D. Decreasing frequency drift noise

Again, frequency drift noise is minimized by heeding the advice on reducing the previous noise source. Because frequency drift noise is proportional to  $k$ , we need a stiffness as small as possible (yet allowing stable oscillation at small amplitudes). A second factor regards temperature stabilization and choosing an operating temperature close to the turnaround temperature of the corresponding quartz crystal orientation.

## VIII. PRACTICAL CONSIDERATIONS REGARDING TIP MOUNTING

Tip mass plays a crucial role in the needle sensor, because an imbalance in the effective mass of the coupled beams reduces  $Q$ . Rychen has analyzed the effect of mass imbalance and found that an imbalance of 1.5% leads to a drop of the  $Q$ -value by 63.5% (Fig. 4.8 in [46]). Therefore, the tip of a needle sensor needs to be very small. Long and thin tips, however, can show significant thermal lateral oscillations and bend strongly under lateral forces. Young's modulus of tungsten is around 400 GPa, thus a square wire with a diameter of 0.01 mm and a length of 0.3 mm has a lateral stiffness of only 22 N/m. In contrast, the qPlus sensor can easily accommodate heavy and more stable tips that can be resharpened more easily, with significant abrasion [50] and even cleaved in situ [51].

## IX. SUMMARY AND OUTLOOK

Concluding, we compared force sensors based on length-extensional resonators and based on quartz tuning forks. We found that in contrast to applications in the literature, the effective spring constant of a needle sensor is actually twice as large as the stiffness of one tine (see eq. 16). We have discussed four types of noise: sensor noise, thermal noise, oscillator noise and frequency drift noise. Surprisingly, the deflection detector noise is independent of

sensor stiffness, because while a stiffer sensor has less frequency shift proportional to  $1/k$ , its deflection signal increases linear with  $k$ . The other three noise sources, however, clearly favor sensors with spring constants around 1 kN/m. The cantilever geometry provides more charge per force than the length extensional geometry. However, the longitudinal outline of the needle sensor is more suited to a space conserving microscope.

## X. ACKNOWLEDGMENTS

We thank Federico de Faria-Elsner, Joachim Welker and Jay Weymouth for writing the software that analyzes the thermal peak and deflection noise densities and we are grateful to Thomas Hofmann and Joachim Welker for providing the data underlying Figure 9.

- 
- [1] G. Binnig, C. F. Quate, Ch. Gerber, *Phys. Rev. Lett.* **56**, 930 (1986).
  - [2] T. R. Albrecht, P. Grutter, H. K. Horne, D. Rugar, *J. Appl. Phys.* **69**, 668 (1991).
  - [3] M. Tortonese, R.C. Barrett, C.F. Quate, *Appl. Phys. Lett.* **62**, 834 (1993).
  - [4] F. J. Giessibl, *Science* **267**, 68 (1995).
  - [5] F. J. Giessibl, *Reviews of Modern Physics* **75**, 949 (2003).
  - [6] F. J. Giessibl, H. Bielefeldt, S. Hembacher, J. Mannhart, *Appl. Surf. Sci.* **140**, 352 (1999).
  - [7] G. Meyer, N.M. Amer, *Appl. Phys. Lett.* **53**, 1045 (1988).
  - [8] U. Gysin, S. Rast, P. Ruff, E. Meyer, D. W. Lee, P. Vettiger, C. Gerber, *Phys. Rev. B* **69**, 045403 (2004).
  - [9] P. Guethner, U. Fischer, and K. Dransfeld, *Appl. Phys. B: Photophys. Laser Chem.* **B48**, 89 (1989).
  - [10] K. Dransfeld, P. Guethner, K. Heitmann *US Patent 5,212,987*, United States Patent and Trademark Office (1993).
  - [11] K. Bartzke, T. Antrack, K.-H. Schmidt, E. Dammann, CH. Schatterny, *International Journal of Optoelectronics* **8**, 669 (1993).
  - [12] K. Bartzke, T. Antrack, K. Besocke, E. Dammann, *German Patent and Trademark Office Patent DE 19513529A1* (1995).
  - [13] F. J. Giessibl, *German Patent and Trademark Office Patent DE 19633546* (1996).

- [14] F. J. Giessibl, *Appl. Phys. Lett.* **73**, 3956 (1998).
- [15] F. J. Giessibl, *Appl. Phys. Lett.* **76**, 1470 (2000).
- [16] F. J. Giessibl, S. Hembacher, H. Bielefeldt, J. Mannhart, *Science* **289**, 422 (2000).
- [17] S. Hembacher, F. J. Giessibl, J. Mannhart, *Science* **305**, 380 (2004).
- [18] F. J. Giessibl, M. Herz, J. Mannhart, *Proc. Natl. Acad. Sci. (USA)* **99**, 12006 (2002).
- [19] S. Hembacher, F. J. Giessibl, J. Mannhart, C.F. Quate *Phys. Rev. Lett.* **94**, 056101 (2005).
- [20] S. Hembacher, F. J. Giessibl, J. Mannhart, *Appl. Surf. Sci.* **188**, 445 (2002).
- [21] M. Ternes, C. Lutz, C.F. Hirjibehedin, F. J. Giessibl, A. Heinrich, *Science* **319**, 1066 (2008).
- [22] L. Gross, F. Mohn, P. Liljeroth, J. Repp, F. J. Giessibl, G. Meyer, *Science* **324**, 1428 (2009).
- [23] L. Gross, F. Mohn, N. Moll, P. Liljeroth, G. Meyer, *Science* **325**, 1110 (2009).
- [24] L. Gross, F. Mohn, N. Moll, G. Meyer, R. Ebel, W.M. Abdel-Mageed and M. Jaspars, *Nature Chemistry* **2**, 821 (2010).
- [25] M. Ternes, C. Gonzalez, C.P. Lutz, P. Hapala, F.J. Giessibl, P. Jelinek, A. Heinrich, *Phys. Rev. Lett.* **106**, 016802 (2011).
- [26] Z. Sun, M.P. Boneschanscher, I. Swart, D. Vanmaekelbergh, P. Liljeroth, *Phys. Rev. Lett.* **106**, 046104 (2011).
- [27] F. J. Giessibl, *Appl. Phys. Lett.* **78**, 123 (2001).
- [28] T. An, T. Eguchi, K. Akiyama, Y. Hasegawa *Appl. Phys. Lett.* **87**, 133114 (2005).
- [29] T. An, T. Nishio, T. Eguchi, M. Ono, A. Nomura, K. Akiyama, Y. Hasegawa *Rev. Sci. Instrum.* **79**, 033703 (2008).
- [30] S. Torbrügge, O. Schaff, J. Rycken *J. Vac. Sci. Technol.* **B28**, C4E12 (2010).
- [31] C.J. Chen, *Introduction to Scanning Tunneling Microscopy*, Oxford University Press, New York, Oxford 1993.
- [32] U. Dürig, J. K. Gimzewski, D. W. Pohl, *Phys. Rev. Lett.* **57**, 2403 (1986).
- [33] F. J. Giessibl, H. Bielefeldt, *Phys. Rev. B* **61**, 9968 (2000).
- [34] Y. Hasegawa, T. Eguchi, T. An, M. Ono, K. Akiyama, T. Sakurai *Jpn. J. Appl. Phys.* **43**, L303 (2004).
- [35] K. Kobayashi, H. Yamada, K. Matsushige, *Rev. Sci. Instrum.* **80**, 043708 (2009).
- [36] T. Eguchi, Y. Hasegawa, *Phys. Rev. Lett.* **89**, 266105 (2002).
- [37] E. Momosaki, Sh. Kogure, pp. 47-60 in *Piezoelectricity*, G.W. Taylor, J.J. Gagnepain, T.R. Meeker, T. Nakamura, L.A. Shuvalov (eds.), Gordon and Breach, New York (1985).

- [38] R. Perez, I. Stich, M.C. Payne, K. Terakura, *Phys. Rev. B* **58**, 10835 (1998).
- [39] T. Hofmann, J. Welker, F.J. Giessibl, unpublished (2011).
- [40] Femto HQA-15M-10T, Femto GmbH, Berlin, Germany.
- [41] Kolibri-Preamplifier, SPECS GmbH, Berlin, Germany.
- [42] Nanonis - SPECS Zurich GmbH, 8005 Zurich, Switzerland.
- [43] Microcrystal product brochure, Micro Crystal AG, Mhlestrasse 14, CH-2540 Grenchen, Switzerland.
- [44] A. Schirmeisen, G. Cross, A. Stalder, P. Grütter, U. Dürig, *New Journal of Physics* **2**, 29 (2000).
- [45] Roger W. Ward, *Constants of Alpha Quartz*, pp. 211-220 in C.Zwick Rosen, B.V. Hiremath, R. Newnham (eds.) *Piezoelectricity*, American Institute of Physics, New York (1992).
- [46] J. Rychen, *Combined Low-Temperature Scanning Probe Microscopy and Magneto-Transport Experiments for the Local Investigation of Mesoscopic Systems*, Diss. ETH No. 14229, Swiss Federal Institute of Technology, Zurich, CH (2001).
- [47] Frederico de Faria Elsner, *Untersuchung der Rauschgrenzen bei der Messung kleinster mechanischer Auslenkungen*, diploma thesis, University of Regensburg, Germany (2010).
- [48] S. Morita, E. Meyer, R. Wiesendanger (eds.), *Noncontact Atomic Force Microscopy*, Springer, New York (2002).
- [49] C. M. Van Vliet, *Physica A* **303**, 421 (2001).
- [50] T. Hofmann, J. Welker, F.J. Giessibl, *J. Vac. Sci. Technol.* **B28**, DOI: 10.1116/1.3294706 (2010).
- [51] T. Wutscher, F.J. Giessibl, *Rev. Sci. Instrum.* **82**, 026106 (2011).